Available online at www.sciencedirect.com
SCIENCE DIRECT®
Finite Elements in Analysis and Design 42 (2005) 130–151
FINITE ELEMENTS IN ANALYSIS AND DESIGN
www.elsevier.com/locate/finel

The propagation problem in longest-edge refinement

José P. Suárez[a,*], Ángel Plaza[b], Graham F. Carey[c]

[a] *Department of Cartography and Graphic Engineering, University of Las Palmas de Gran Canaria, Spain*
[b] *Department of Mathematics, University of Las Palmas de Gran Canaria, Spain*
[c] *Institute for Computational Engineering and Sciences (ICES), The University of Texas at Austin, TX, USA*

Received 14 September 2004; received in revised form 14 May 2005; accepted 9 June 2005
Available online 28 July 2005

Abstract

Two asymptotic properties that arise in iterative mesh refinement of triangles are introduced and investigated. First, we provide theoretical results showing that recursive application of uniform four triangles longest-edge (4T-LE) partition to an arbitrary unstructured triangular mesh produces meshes in which the triangle pairings sharing a common longest edge asymptotically tend to cover the area of the whole mesh. As a consequence, we prove that for a triangle, the induced exterior conforming refinement zone extends on average to a few neighbor adjacent triangles. We determine the asymptotic extent of this propagating path and include results of supporting numerical experiments with uniform and adaptive mesh refinement. Similar behavior and LE propagation from a four triangle self similar (4T-SS) local subdivision alternative is analyzed and compared numerically. Hybrid 4T-LE and 4T-SS LE schemes are also considered. The results are relevant to mesh refinement in finite element and finite volume calculations as well as mesh enhancement in Computer Graphics and CAGD.

Keywords: Mesh refinement; Longest edge; Propagation path

1. Introduction

Certain longest-edge (LE) local refinement algorithms [1,2] guarantee the construction of non-degenerate and smooth unstructured triangulations. In these schemes the longest edges are progressively

* Corresponding author. Tel.: 34 928 457268; fax: 34 928 451872.
E-mail addresses: jsuarez@dcegi.ulpgc.es (J.P. Suárez), aplaza@dmat.ulpgc.es (A. Plaza), carey@cfdlab.ae.utexas.edu (G.F. Carey).

0168-874X/$ - see front matter © 2005 Elsevier B.V. All rights reserved.
doi:10.1016/j.finel.2005.06.005

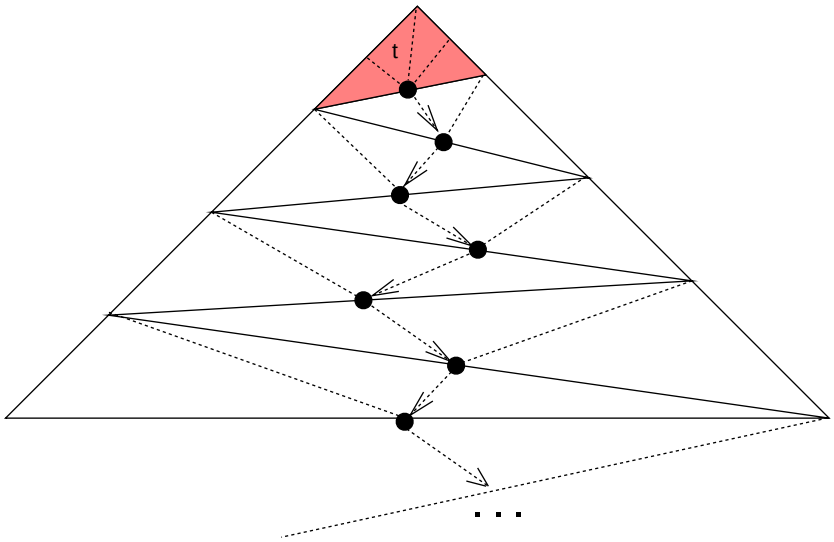

Fig. 1. An extreme case in LE based refinement propagation. The dependencies in the propagation when refining t are indicated by arrows. Additional dashed lines are introduced to complete the new triangulation.

bisected and hence all angles in subsequent refined triangulations are greater than or equal to half the smallest angle in the initial triangulation [2]. However, the extent of secondary refinements induced in neighboring elements by the initiating element subdivision is not known [1,3]. In fact, one can construct pathological cases where refinement of a single element propagates through the entire mesh (Fig. 1). However, in practice, the average extent of the propagation paths or zones of secondary refinement at each adaptive refinement stage are obviously the significant property in question. If the averages are small, then the transition zones tend to involve only a few neighbor elements. Secondary refinement provides more gradual transition between refined and unrefined elements and promotes mesh quasi-uniformly. Our main goal here is to explore secondary refinement and related issues concerning the 'quality' of the resulting mesh.

We proceed as follows: First, we provide both theoretical results and empirical evidence showing that recursive application of a uniform LE refinement scheme to an arbitrary unstructured triangular mesh produces 'balanced' meshes in which triangle pairings that share a common longest edge asymptotically tend to cover the area of the whole mesh. In so doing we show that the refinement scheme can be formulated and implemented to improve an initial inferior mesh. Both LE and hybrid LE-similar local element subdivisions are considered. One consequence is that the average propagation zone for each triangle is reduced in each uniform refinement stage, and asymptotically approaches five neighbor triangles.

A similar behavior is observed for recursive local adaptive mesh refinement. However, the extent of the adjacent secondary refinement depends on the nature of the local refinement. This implies that the uniform LE refinement strategy can be used to advantage in improving an initial mesh and prior to invoking a local adaptive mesh refinement algorithm. The AMR scheme can exhibit longer average propagation zones and larger paths which act to enforce a more gradual mesh transition but still exhibit a similar behavior. Numerical studies with uniform and local AMR illustrate the behavior. Although our focus here is on unstructured two-dimensional (2-D) triangulations, the extension of these ideas to three-dimensional (3-D) is briefly considered in the final section and some related open problems posed.

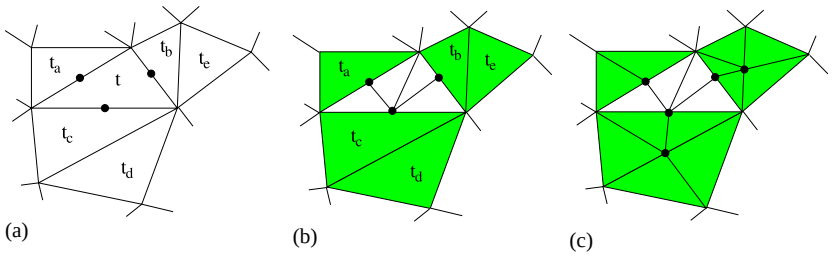

Fig. 2. (a) Edgde bisection for refining triangle *t*, (b) 4T-LE refinement of *t* and induced propagation in shaded color, (c) secondary refinement.

1.1. LE refinement and the propagation problem

Frequently, mesh refinement is divided into two types: *uniform* and *local*: Uniform implies the refinement of all triangles in a mesh, usually following a specified local subdivision pattern. If the refinement is made locally for only a single triangle or a sub-group of triangles, then the refinement is local. Local refinement of triangular meshes involves two main tasks. The first is the local partition of the target triangles and the second is the propagation to successive neighbor triangles to preserve mesh conformity. Several approaches for partitioning triangles have been studied. The simplest is *Bisection* into two subtriangles by connecting the midpoint of one of the edges to the opposite vertex. If the LE is chosen for the bisection, then this is called *longest edge bisection*. The *four-triangles longest-edge partition* (*4T-LE*) bisects a triangle into four subtriangles as follows: the original triangle is first subdivided by its longest edge as before and then the two resulting triangles are bisected by joining the new midpoint of the longest edge to the midpoints of the remaining two edges of the original triangle. An alternative strategy is to connect the midpoints of the edges by lines parallel to the edges. This again yields four subtriangles, each being similar to the original parent triangle and therefore inheriting its shape quality (good or bad). This latter subdivision is referred to as the 'natural' or self-similar (SS) pattern. The local element 4T-LE and the 4T-SS pattern can be interchanged easily by a local interior 'edge swap'. As a hybrid variant local 4T-LE and 4T-SS subdivision can obviously be deployed independently on cells within each uniform refinement step.

However, we are ultimately interested in local adaptive mesh refinement (AMR) with conforming meshes. Local subdivision of the 'target' element by 4T-LE or 4T-SS introduces new midedge nodes on the element boundary. In order to ensure conformity of the resulting mesh, the refinement is extended to additional triangles and here we consider a progressive longest edge approach. These adjacent LE partition patterns always bisect the adjacent triangle by the midpoint of the LE and then, if necessary, one or two of the resulting subtriangles are also bisected, as indicated in Fig. 2. We refer to these additional triangles as the *propagation* zone. Note that the corresponding 4T-SS pattern can be obtained simply by an interior edge swap applied to the initiating 4T-LE bisector with no change to the propagation zone shaded in the figure.

2. Pair-balancing degree in recursive 4T-LE refinement

Our first goal is to prove that recursive application of uniform 4T-LE partition to an arbitrary unstructured triangular mesh produces meshes in which the triangle pairings that share a common longest edge

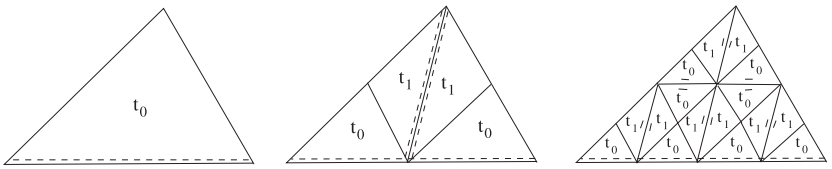

Fig. 3. Repeated 4T-LE partition of a right or acute triangle. (Here and in subsequent figures we mark the LE with a dashed line.)

asymptotically tend to cover the area of the mesh. We will then use this property to show that the mean associated propagation zone asymptotically approaches a small value. We show that similar results apply for 4T-SS subdivision of the initial triangle followed by LE propagation to neighbors. A similar behavior is exhibited in recursive AMR and we explore this variation with an associated hybrid algorithm.

Definition 1 (*pair of terminal triangles*). Two neighbor triangles (t, t^*) will be called a 'pair' of terminal triangles if they share a common longest edge. If a triangle t does not belong to a pair of terminal triangles, t is said to be a 'single' triangle.

Definition 2 (*pair-balanced mesh*). Triangulation τ is said to be pair-balanced if it is comprised of pairs of terminal triangles.

Definition 3 (*pair-balancing degree*). Let τ contain N triangles of which T triangles are in pairs of terminal triangles. Then, the pair-balancing degree of τ, noted as $B(\tau)$, is defined as

$$B(\tau) = \frac{T}{N}. \tag{1}$$

Remark. Obviously, $0 \leqslant B(\tau) \leqslant 1$ and in the case $B(\tau) = 1$, the mesh is pair-balanced. If τ is such that the pair-balancing degree is 0, then the conformity process when refining any triangle $t_0 \in \tau$ extends to the boundary of τ (recall Fig. 1).

To demonstrate that recursive uniform 4T-LE refinement introduces meshes with relatively more pairs of terminal triangles for any arbitrary triangular mesh we consider right, acute and obtuse triangles respectively. We begin in the next proposition with the right and acute triangle cases:

Proposition 1 (*right and acute triangle cases*). *The application of the 4T-LE partition to an initial right or acute triangle t_0 produces two new single triangles similar to the original one* (*located at the longest edge of t_0*) *and a pair of terminal triangles t_1. These triangles t_1 are also similar to the original one in the case of right triangle t_0, and they are similar to each other but non-similar to the initial one in the case of acute triangle t_0* (*see Fig.* 3).

The obtuse triangle case offers a different situation:

Proposition 2 (*obtuse triangle case*). *The application of the 4T-LE partition to an initial obtuse triangle t_0, produces two new single subtriangles similar to the original one (located at the longest edge of t_0) and a pair of subtriangles t_1. These subtriangles t_1 are either*: 1. *Are a pair of similar terminal triangles,*

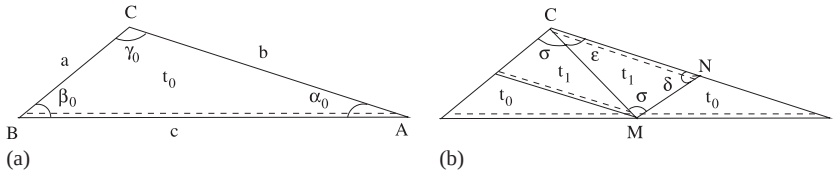

Fig. 4. (a) Type 2 obtuse triangle t_0 and (b) 4T-LE partition of t_0.

as in Fig. 3 (b) (*t_0 is said to be a Type* 1 *obtuse triangle*), *or* 2. *A pair of similar single triangles, as in Fig.* 4 (b) (*t_0 is said to be a Type* 2 *obtuse triangle*).

A proof of Propositions 1 and 2 can be found in [4].

Remark. It should be noted that the 4T-LE partition always produces two new single triangles similar to the original one (located at the longest edge of t_0) and excepting for Type 2 obtuse triangles, a pair of terminal triangles (similar or non similar to the original one). Moreover, in this scenario, the single triangles generated by the iterative 4T-LE partition are those located at the longest edge of the initial triangle (see Fig. 3).

Proposition 3. *Let t_0 be an initial obtuse triangle in which the 4T-LE partition is iteratively applied. Then a* (*finite*) *sequence of dissimilar triangles, one per iteration, is obtained*: $\{t_0, t_1, t_2, \ldots, t_M, t_{M+1}\}$ *where triangles $t_0, t_1, \ldots, t_{M-1}$ are obtuse, triangle t_M is not obtuse, and the 4T-LE partition of t_M produces* (*at most*) *one new obtuse triangle t_{M+1}. From this point on, no new dissimilar triangles are produced* [5].

It follows that the iterative 4T-LE partition of an obtuse triangle produces a finite sequence of 'better' triangles in the sense shown in the following diagram [6] until triangle t_M becomes nonobtuse:

$$\begin{array}{ccccccc}
t_0 & \rightarrow & t_1 & \rightarrow & t_2 & \rightarrow \ldots \rightarrow & t_M \\
\text{(obtuse)} & & \text{(obtuse)} & & \text{(obtuse)} & & \text{(nonobtuse)} \\
\alpha_0 & & \alpha_1 > \alpha_0 & & \alpha_2 > \alpha_1 & & \alpha_M > \alpha_{M-1} \\
\gamma_0 & & \gamma_1 \leqslant \gamma_0 - \alpha_1 & & \gamma_2 \leqslant \gamma_1 - \alpha_2 & & \gamma_M \leqslant \gamma_{M-1} - \alpha_M,
\end{array}$$

where α_i, and γ_i, are respectively the smallest and the largest angles of triangle t_i. The arrow emanating from triangle t_i to triangle t_{i+1} means that the (first) 4T-LE partition of triangle t_i produces the new dissimilar triangle t_{i+1}.

The process described in the preceding diagram inevitably results in one of the following situations [6]:

$$\begin{array}{lccccccc}
(1) & t_{M-1} & \rightleftharpoons & t_M & & & & \gamma_{M-1} + \gamma_M = \pi, \\
 & \text{obtuse} & & \text{nonobtuse} & & & & \\
(2) & t_{M-1} & \rightarrow & t_M\circlearrowleft & & & & \gamma_M = \pi/2, \\
 & \text{obtuse} & & \text{right-angled} & & & & \\
(3) & t_{M-1} & \rightarrow & t_M & \rightleftharpoons & t_{M+1} & & \gamma_M + \gamma_{M+1} = \pi. \\
 & \text{obtuse} & & \text{nonobtuse} & & \text{obtuse} & &
\end{array}$$

The number of dissimilar triangles generated, k, satisfies $k = M + 1$, for the cases (1) and (2) of the previous diagram, or $k = M + 2$ for case (3). The size of k depends on the shape of the initial triangle (see [5]).

In view of the previous properties, we have:

Proposition 4. *Let $\Gamma = \{\tau_0, \tau_1, \ldots, \tau_n\}$ be a sequence of nested meshes obtained by repeated application of 4T-LE partition to the previous mesh. Then, the pair-balancing degree of the meshes tends to* 1 *as* $n \to \infty$.

Proof. It suffices to prove the result for the case in which the initial mesh τ_0 only contains a single triangle t_0. Then, the number of generated triangles associated with the 4T-LE partition at refinement stage n is

$$N_n = 4^n. \tag{2}$$

First, we prove the proposition for initial right, acute, and Type 1 obtuse triangles. In this situation, the number of triangles in pairs of terminal triangles T_n generated at stage n of uniform 4T-LE partition satisfies

$$T_n = 4T_{n-1} + 2(N_{n-1} - T_{n-1}) = 2(T_{n-1} + N_{n-1}) \tag{3}$$

with $N_0 = 1$ and $T_0 = 0$.

Solving the recurrence relations (2) and (3) we get

$$T_n = 4^n - 2^n. \tag{4}$$

Therefore,

$$\lim_{n\to\infty} B(\tau_n) = \lim_{n\to\infty} \frac{T_n}{N_n} = 1.$$

To complete the proof, we now consider the case of an initial Type 2 obtuse triangle t_0. Table 1 presents the number of distinct types of triangles generated by the 4T-LE iterative refinement of t_0. We denote by t_j^n the number of triangles of similarity class t_j, $j = 0, 1, 2, \ldots, k$ at refinement stage n. For example,

Table 1
Triangle evolution in the 4T-LE partition

Ref.	0	1	2	3	4	$\cdots$	k	$\cdots$	n
t_0	1	2	4	8	16	$\cdots$	t_0^k	$\cdots$	t_0^n
t_1		2	8	24	64	$\cdots$	t_1^k	$\cdots$	t_1^n
t_2			4	24	96	$\cdots$	t_2^k	$\cdots$	t_2^n
t_3				8	64	$\cdots$	t_3^k	$\cdots$	t_3^n
t_4					16	$\cdots$	t_4^k	$\cdots$	t_4^n
$\vdots$						$\ddots$	$\vdots$	$\cdots$	$\vdots$
t_k							t_k^k	$\cdots$	t_k^n

after the second refinement 4 triangles are similar to t_0, 8 triangles similar to t_1 and 4 new triangles similar to t_2.

For each triangle of class t_{j-1} at stage $n-1$ of refinement, there are obtained two triangles of class t_{j-1} and two triangles of class t_j at stage n of refinement. This implies that the number of triangles of similarity class t_j, $j=0,1,2,\ldots,k$ at stage n of refinement t_j^n, satisfy the recurrence relation:

$$t_j^n = 2(t_j^{n-1} + t_{j-1}^{n-1}), \quad j = 1,2,3,\ldots,k. \tag{5}$$

The solution to Eq. (5) with initial condition $t_0^0 = 1$ can be easily expressed in terms of binomial coefficients as

$$t_j^n = 2^n \binom{n}{j}. \tag{6}$$

On the other hand, the iterative 4T-LE partition of any obtuse triangle t_0 produces a finite number of distinct (up to similarity) triangles, t_j^i, $0 < j \leqslant k$. After $i = k$ refinement stages there will no longer be distinct new generated triangles different from those already generated. Therefore, the number of triangles in pairs of terminal triangles T_n after the k refinement stage with $n > k$ satisfy

$$T_n \geqslant 2^n \sum_{m=k}^{n} \binom{n}{m}.$$

It follows that

$$B(\tau_n) \geqslant \frac{2^n \sum_{m=k}^{n} \binom{n}{m}}{2^n \sum_{m=0}^{n} \binom{n}{m}} = \frac{\sum_{m=k}^{n} \binom{n}{m}}{2^n}.$$

Taking limits

$$\lim_{n\to\infty} B(\tau_n) \geqslant \lim_{n\to\infty} \frac{\sum_{m=k}^{n} \binom{n}{m}}{2^n}.$$

Since

$$\sum_{m=k}^{n} \binom{n}{m} = 2^n - \sum_{m=0}^{k-1} \binom{n}{m} \geqslant 2^n - \binom{n}{k-1} k$$

we have

$$\lim_{n\to\infty} B(\tau_n) \geqslant \lim_{n\to\infty} \frac{2^n - \binom{n}{k-1} k}{2^n} = 1$$

but, by definition, $B(\tau_n) \leqslant 1$, so $\lim_{n\to\infty} B(\tau_n) = 1$. □

Self-similar (*4T-SS*) *partition*: It is even simpler to show that the pair-balancing degree of the refined meshes tends to 1 in the case where local SS subdivisions are applied. Once again, the partition produces four sub-triangles with two of them having their longest edges on the longest edge of the parent triangle and the other two being always a pair of terminal triangles. The next proposition states the result corresponding to the preceding 4T-LE partition in Proposition 4.

Proposition 5. *Let* $\Gamma = \{\tau_0, \tau_1, \ldots, \tau_n\}$ *be a sequence of nested meshes obtained by repeated application of 4T-SS partition to the previous mesh. Then, the pair-balancing degree of the meshes tends to* 1 *as* $n \to \infty$.

Proof. The number of triangles in pairs of terminal triangles T_n generated at stage n of uniform *SS* partition satisfies

$$T_n = 4T_{n-1} + 2R_{n-1}, \tag{7}$$

where R_{n-1} are the number of single triangles in the stage $(n-1)$.

The number of single triangles R_n is

$$R_n = 2R_{n-1} \tag{8}$$

as only two triangles remain single from a triangle partition.

Solving the recurrence relations (7) and (8) we get

$$T_n = 4^n T_0 - 2^n R_0 = 4^n (T_0 + R_0) - 2^n R_0 \tag{9}$$

and taking limits to calculate the pair-balancing degree:

$$\lim_{n\to\infty} B(\tau_n) = \lim_{n\to\infty} \frac{T_n}{N_n} = 1. \quad \square$$

Remark. It follows trivially that recursive application of hybrid 4T-LE and 4T-SS refinement to subsets of elements in an initial mesh will also approach an asymptotically balanced grid.

In the next section we use the above property to show that the propagation in local LE refinement from an arbitrary cell asymptotically extends on average to a few neighbor adjacent triangles as this uniform recursive mesh sequence evolves. We then examine the average secondary refinement behavior of recursive local adaptive refinement schemes based on longest edge bisection in several numerical experiments.

3. Propagation properties

Assume we consider any mesh generated in the *uniform* refinement sequence defined in Section 2. We seek to study the behavior of the propagation zone if local refinement were to be subsequently applied to *any* element of such a mesh. We do this by computing the zone for each element and determining the mean and standard deviation. This permits a statistical study of the asymptotic behavior of the propagation zone. Recall that the longest edge neighbor of a triangle t_0 is the neighbor triangle t_1 which shares with t_0 the longest edge of t_0. The longest edge propagation path (LEPP) of a triangle t_0 is the ordered finite

list of all adjacent triangles $LEPP(t_0) = \{t_0, t_1, \ldots, t_n\}$ such that t_i is the LE neighbor triangle of t_{i-1}. A triangle t is said to be a *boundary* triangle if t has an edge coincident with the boundary $\partial\Omega$ of the domain Ω. Otherwise, t is an interior triangle. For any triangle t_0, where $LEPP(t_0) = \{t_0, \ldots, t_{n-1}, t_n\}$ then for triangle t_n either: (i) t_n has its LE coincident with the boundary or (ii) t_{n-1} and t_n are a pair of terminal triangles [7].

When refining a triangle $t \in \tau$, the propagation zone of t is the set of triangles in $\tau^* = \tau - t$ that need to be refined due to the conformity process for t. We define $M1(t)$ to be the extent of the propagation refinement zone for triangle t, in number of triangles. Thus, for each $t \in \tau$, $M1(t)$ is the sum of the lengths of the LEPP′s of the neighbors of t in the mesh $\tau^* = \tau - t$.

Fig. 1 shows that it always is possible to construct meshes in which $M1(t)$ is $\mathcal{O}(N)$, where N is the number of elements. Here, the average of $M1$ is

$$\mu(M1) = \frac{\sum_t M1(t)}{N} = \frac{\sum_{k=0}^{N-1} k}{N} = \frac{\frac{N-1}{2} \cdot N}{N} = \frac{N-1}{2}.$$

Since the conformity process extends at most by the three edges of t the propagation defines at most three lists of ordered triangles. Let $M2(t)$ be the maximum number of triangles of the three resulting lists. For example, in Fig. 2, $M2(t) = 2$ because the maximum number of triangles among $\{t_b, t_e\}$, $\{t_c, t_d\}$, $\{t_a\}$ is 2. Clearly $M1(t) = 5$ in Fig. 2.

Proposition 6. *Let τ be pair-balanced. Then, for each interior triangle $t \in \tau$, $M1(t) = 5$ and $M2(t) = 2$.*

Proof follows trivially from the Definition of $B(\tau)$.

Remark. Note that if the 4T-LE partition is used to refine a given triangle t, then the LEPP's of the neighbor triangles of t in the mesh $\tau^* = \tau - t$ provide the lists of triangles to be refined (see Fig. 2). As a consequence, the LEPP's provide the main adjacency lists used by the 4T-LE local refinement procedure.

In the present work we are particularly interested in the properties of the averages $\mu(M1)$ and $\mu(M2)$ as the mesh is refined. Let us first consider 4T-LE subdivision.

Proposition 7. *For iterative application of 4T-LE uniform refinement to an initial triangular mesh τ_0, the means of $M1$ and of $M2$ tend to 5 and 2 respectively, as the number of refinements increase and the rate of convergence is linear.*

Proof. If the initial mesh is pair-balanced the result is trivial. Therefore, let us consider the case where the initial mesh contains single triangles. In any subsequent mesh we have pairs of terminal triangles and single triangles.

First, we prove the proposition for an initial mesh of right, acute, or Type 1 obtuse single triangles arranged in such a way that $M1$ and $M2$ have the largest possible magnitudes. That is, all the single triangles constitute a unique LEPP. Fig. 5 (a) reproduces such a possible situation within a mesh. After a few refinement steps it is observed that new single triangles are located at the longest edges of the initial triangles and balanced pairs are formed elsewhere. We represent in bold the longest edges of single triangles as shown in Fig. 5 (d) and refer to this line diagram as a *polyline*.

Once this polyline is established, the single triangles satisfy $6 \leqslant M1 \leqslant 7$ and $2 \leqslant M2 \leqslant 3$. For a triangle in a terminal pair we get $5 \leqslant M1 \leqslant 6$ and $2 \leqslant M2 \leqslant 3$ if it has a vertex on the polyline, or $M1 = 5$ and

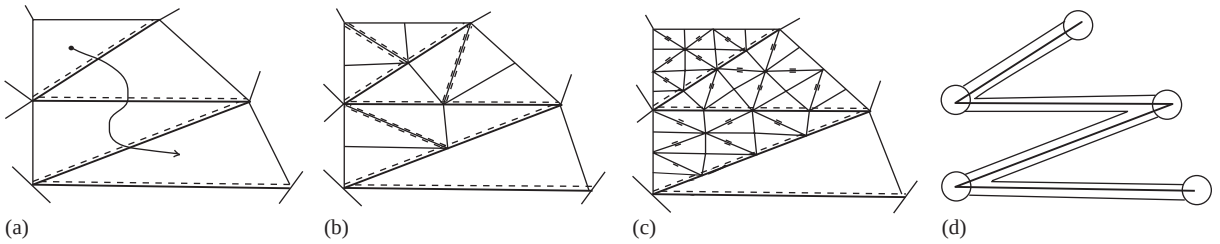

Fig. 5. (a) Single triangles forming a LEPP, (b)–(c) 4T-LE refinement of triangulation in (a), (d) Polyline defined by longest edges of triangles in (a).

$M2 = 2$ otherwise. After n refinement steps, the number of single triangles is $X_n = 2^n X_0$ and the number of total triangles is $N_n = 4^n N_0$. Using these inequalities, upper and lower bounds for the average $\mu(M1)$ are

$$\frac{6X_n + 5(N_n - X_n)}{N_n} \leqslant \mu(M1) \leqslant \frac{7X_n + 6X_n - 5(N_n - 2X_n)}{N_n}.$$

That is,

$$5 + \frac{X_n}{N_n} \leqslant \mu(M1) \leqslant 5 + \frac{3X_n}{N_n}. \tag{10}$$

Similarly for $\mu(M2)$:

$$\frac{2X_n + 2(N_n - X_n)}{N_n} \leqslant \mu(M2) \leqslant \frac{3 \cdot 2X_n + 2(N_n - 2X_n)}{N_n}$$

and simplifying,

$$2 \leqslant \mu(M2) \leqslant 2 + 2\frac{X_n}{N_n}. \tag{11}$$

In the above expressions $X_n/N_n = X_0/2^n N_0 \leqslant 1/2^n$, so taking limits, the means of $M1$ and of $M2$ tend to 5 and 2, respectively, as the number of refinements n tends to infinity. Moreover, the error $|2 - \mu(M(2))|/2 \leqslant 2^{-n}$ so the error bound halves at each step.

To complete the proof, we should also consider the case of Type 2 obtuse triangles. As pointed out after Proposition 3, in repeated *4T-LE* refinement the largest angles of Type 2 obtuse triangles decrease (excluding single triangles on the polyline), and after a finite number of partitions no new triangles appear. Hence, the above proof for right or acute triangle cases then applies. □

Proposition 8. *For iterative application of 4T-SS uniform refinement to an initial triangular mesh* τ_0*, the means of* $M1$ *and of* $M2$ *tend to* 5 *and* 2 *respectively, as the number of refinements increase.*

Proof. It follows trivially from the fact that the 4T-SS uniform refinement to an initial triangular mesh τ_0 does not include any single elements other than those sharing their longest edge with the single elements of mesh τ_0. Therefore, inequalities (10) and (11) can be also applied in this case. □

3.1. AMR implications

The preceding discussion deals with the asymptotic behavior under uniform refinement as implied in Figs. 3 and 4. For this uniform refinement case it is clear that the improvement in mesh quality and non-degeneracy are important. The propagation path properties are not otherwise relevant to the refinement process or efficiency of a simulation in this situation. However, these propagation path ideas are of practical interest when one considers the efficiency of LE local refinement in AMR algorithms. Obviously, refining a single triangle can generate large values for $M1$ and $M2$. In AMR however, one typically refines a small percentage of the elements at each refinement step and several AMR stages are carried out during the simulation so we are again dealing with recursive refinement of some elements. Also note that repeated AMR stages often are focused in specific subregions such as layer regions or near singularities where the solution is changing significantly. Hence the behavior locally resembles a quasi-uniform refinement and we expect the behavior under uniform refinement to be relevant.

It is clear that the AMR situation for $\mu(M1)$, $\mu(M2)$ can not be analyzed as rigorously as in the previous uniform case since the refinement is not fully recursive. In AMR we generate an unbalanced refinement tree with, generally, some elements at root level zero, some at the next level one, and so on to the finest refinement level. These active elements are the 'leaves' of the tree and the highest level leaves will be the result of multiple refinements applied through the previous levels. The behavior of $\mu(M1)$ and $\mu(M2)$ in the highly refined subregions is therefore anticipated to approach the asymptotic values seen in the earlier treatment of uniform refinements whereas the behavior on the level zero and level one mesh subregions will be similar to the pre-asymptotic behavior. The average 'behavior' will be intermediate and depend on the extent of refinement. This further suggest that, in practice, one might encourage beginning with as coarse a mesh as possible followed by, say, three uniform LE or hybrid refinements before activating AMR. (A hybrid refinement is one in which local 4T-LE and 4T-SS are selectively applied). Of course, if one can improve the coarse mesh by a Delaunay scheme or by mesh smoothing to produce an initial mesh of better shape quality, then this will be beneficial. Hence we emphasize we are not advocating one improvement scheme over another but merely studying the behavior of one approach.

4. Numerical experiments

In this section we present numerical results to examine the behavior of B, $\mu(M1)$ and $\mu(M2)$ for several test cases and compare these results with the preceding theoretical predictions, (eg. in Propositions 4 and 7).

4.1. Uniform refinement case

4.1.1. Pentagon domain

Consider the irregular mesh in a pentagon shown in Fig. 6(a). Except for the interior central five elements, all triangles are slender with high aspect ratio. The mean of the minimum angles and of the maximum angles are 9.18° and 120.41°, respectively, and $B(\tau_0) = 0$.

Three refined meshes obtained by uniform 4T-LE subdivision are shown in Fig. 6(b)–(d). Table 2 reports the means and standard deviations of $M1$ and $M2$ and the evolution of the balancing degree computed after each uniform refinement step. As expected, $\mu(M1) \to 5$, $\mu(M2) \to 2$, and the standard deviations

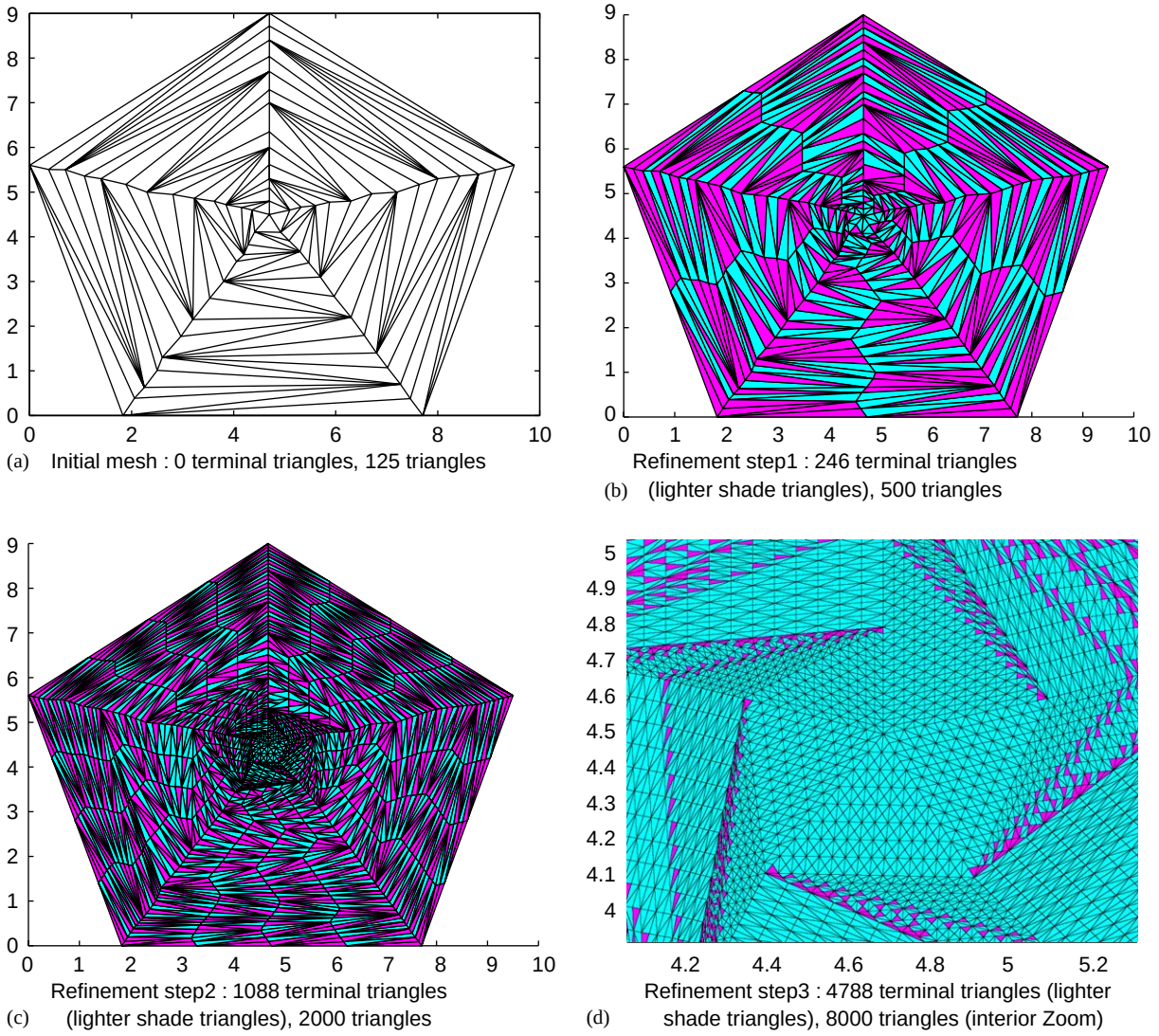

Fig. 6. Pentagonal mesh. Uniform 4T-LE refinement. (a) Initial mesh: 0 terminal triangles, 125 triangles, (b) Refinement step 1:246 terminal triangles (lighter shade triangles), 500 triangles, (c) Refinement step 2: 1088 terminal triangles (lighter shade triangles), 2000 total triangles, (d) Refinement step 3: 4778 terminal triangles (lighter shade triangles), 8000 triangles (interior zoom).

reduce correspondingly. In addition the balancing degree tends to 1 when the number of refinements increases.

4.1.2. Square domain

The highly skewed initial grid in Fig. 7(a) was uniformly refined using the 4T-LE scheme. The first three refinement patterns are given in Figs. 7(b)–(d) and more complete details are provided in Table 3.

Table 2
Balancing degree (B) and $M1$, $M2$ statistics for the refinement of the pentagonal mesh. Average (μ) and standard deviation (σ)

R	N	B	$\mu(M1)$	$\mu(M2)$	$\sigma(M1)$	$\sigma(M2)$
0	125	0	26.544	14.392	16.569	7.156
1	500	0.49200	6.910	3.800	2.204	1.668
2	2000	0.54400	6.200	3.048	1.699	1.103
3	8000	0.59725	5.997	2.831	1.553	0.883
4	32 000	0.66375	5.482	2.412	1.122	0.800
5	128 000	0.81230	5.370	2.204	0.947	0.757

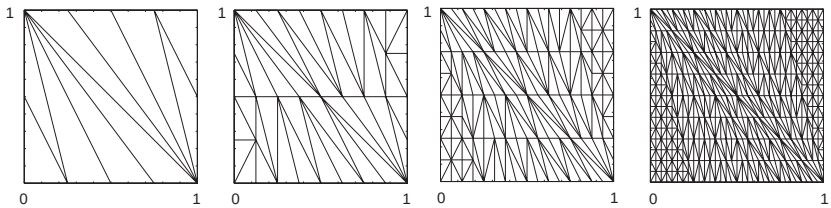

Fig. 7. Square domain: Initial mesh and four uniform 4T-LE refinements.

Table 3
Square domain. 4T-LE refinement. Balancing degree (B) and $M1$, $M2$ statistics for the mesh sequence. Averages (μ) and standard deviation (σ)

R	N	B	$\mu(M1)$	$\mu(M2)$	$\sigma(M1)$	$\sigma(M2)$
0	10	0.2000	3.8000	3.0000	1.2293	1.4907
1	40	0.6000	4.6500	2.6000	1.9553	1.2969
2	160	0.7000	5.0375	2.5000	1.6132	0.8687
3	640	0.7750	5.2062	2.4031	1.3845	0.7143
4	2560	0.8375	5.2203	2.3062	1.1161	0.6009
5	10 240	0.8875	5.1807	2.2172	0.8874	0.5028
6	40 960	0.9102	5.1316	2.1465	0.7007	0.4139
7	163 840	0.9423	5.0027	2.0121	0.4608	0.4579

This square case was repeated using 4T-SS uniform refinement and the results are given in Table 4. Obviously there is no improvement in local element shape quality but the increase in balancing degree implies that any *subsequent* local AMR will again induce LE propagation paths with good average properties.

Next we consider the application of a hybrid 4T-LE and 4T-SS iterative uniform refinement to the mesh in Fig. 7(a): 4T-LE is applied to right/obtuse triangles and 4T-SS to acute triangles at each uniform stage. Results similar to Table 4 are obtained (not shown).

Table 4
Square domain. 4T-SS refinement. Balancing degree (B) and $M1$, $M2$ statistics for the mesh sequence. Average (μ) and standard deviation (σ)

R	N	B	$\mu(M1)$	$\mu(M2)$	$\sigma(M1)$	$\sigma(M2)$
0	10	0.2000	3.8000	3.0000	1.2293	1.4907
1	40	0.6000	4.6000	2.3500	2.2280	1.1668
2	160	0.8000	4.8000	2.1875	1.5573	0.6558
3	640	0.9000	4.9000	2.0969	1.0974	0.3956
4	2560	0.9500	4.9500	2.0492	0.7752	0.2530
5	10 240	0.9750	4.9750	2.0248	0.5479	0.1688
6	40 960	0.9813	4.9875	2.0125	0.3874	0.1156
7	163 840	0.9971	4.9917	2.0023	0.1231	0.0912

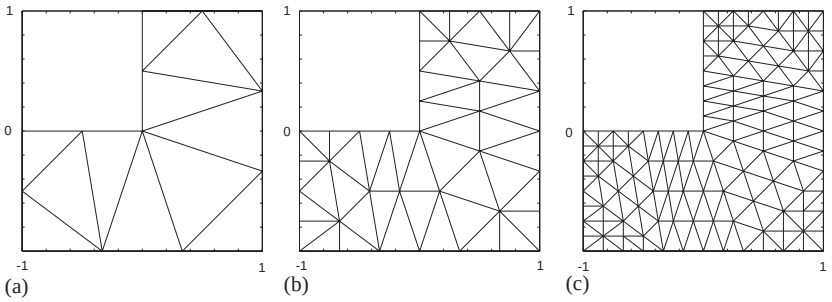

Fig. 8. Hybrid 4T-LE - 4T-SS uniform refinement.

Table 5
Square domain. Hybrid 4T-LE - 4T-SS. Balancing degree (B) and $M1$, $M2$ statistics for the refinement of the mesh (Figs. 8). Average (μ) and standard deviation (σ)

R	N	B	$\mu(M1)$	$\mu(M2)$	$\sigma(M1)$	$\sigma(M2)$
1	12	0.4833	4.0833	3.2500	1.6214	1.7123
2	48	0.7416	6.7500	4.7292	3.6349	3.3373
3	192	0.8708	5.7604	3.1458	2.7846	2.0567
4	768	0.9354	5.6771	2.8451	2.4000	1.9447
5	3072	0.9671	5.5052	2.5615	2.0614	1.6988
5	12 288	0.9915	5.4012	2.2350	1.7329	1.7214

4.1.3. L-shaped domain

Here we consider a case where the initial coarse mesh is the Delaunay triangulation of well-shaped triangles in Fig. 8(a). The subsequent meshes in Fig. 8 employ 4T-LE in obtuse triangles and 4T-SS in acute/right triangles as before. In this case most of the refinement is by the SS pattern. The results in Table 5 for the hybrid scheme are very similar to those obtained by exclusive use of 4T-SS (not shown).

Next we consider the non-uniform refinement case.

4.2. Adaptive refinement studies

The previous studies for uniform refinement via 4T-LE and 4T-SS subdivision lead to meshes with balancing degree approaching 1 as the mesh is repeatedly refined. As seen in the analysis and numerical studies, the averages $\mu(M1)$ and $\mu(M2)$ approach 5 and 2, respectively. This implies that local refinement of a cell will, on average, extend through only a few local elements in such a situation.

In some sense this uniform refinement scenario provides a favourable limit since it leads to balanced meshes consisting only of terminal pairs having the above small propagation zones. Non-uniform refinement strategies will clearly lead to a departure from this optimal propagation behavior and the extent of the departure will clearly depend on the nature of the non-uniform refinement. We consider the most relevant cases below.

4.2.1. Uniform refinement in a subregion

The first case is uniform refinement of a subregion or subregions. This is of interest in certain algorithms, such as those encountered with so-called Shishkin grids for boundary-layer problems [8,9] and for 'windowing' or 'rezoning' subgrids in a region of particular interest. Analogous ideas arise in 'overset' or 'chimera' patches, [10] but in the present instance we assume grid conformity between the subregion fine grid and the exterior coarse grid.

In this subregion case the uniform refinement of a well-balanced subgrid will generate average values that obviously have the same subregion limits as noted above but there will be additional propagation into the grid exterior to the subregion. Since the subregion interface is lower dimensional, the relative effect of this exterior propagation will diminish as uniform refinement of the subregion interior proceeds. This behavior is illustrated graphically in Fig. 9 for uniform refinement of interior subdomains contained in a background mesh of the Gran Canaria Island.

The average values $\mu(M1)$ and $\mu(M2)$ for the entire mesh converge to 5 and 2, respectively, as one might expect since the subregion grid ultimately dominates the process.

4.3. Progressive AMR cases

In practice, we generally seek to use as few cells as possible in a well-graded mesh that is constructed by a more local adaptive refinement process in which a small subset of elements are refined and then a further subset of these are refined and so on. For example, one might expect to refine a fixed fraction of the cells at each refinement step. Often the associated refinement subregions are nested approximately as the solution in a boundary layer region or near a singular point is being resolved. In such cases the balancing degree B, $\mu(M1)$ and $\mu(M2)$ are slightly inferior relative to the fixed subregion case above. Another AMR strategy is to refine those elements having a computable local error indicator above a specified tolerance level. Here the number of cells to be refined can not be specified in advance and in the extreme cases one might have to refine uniformly (all cells have larger indicators) or only one cell may be targeted for refinement. Generally, there will again be a subset of elements to be refined in subregions where the error is too large but the size of the subset may vary significantly as refinement proceeds. The behavior is best illustrated through an example.

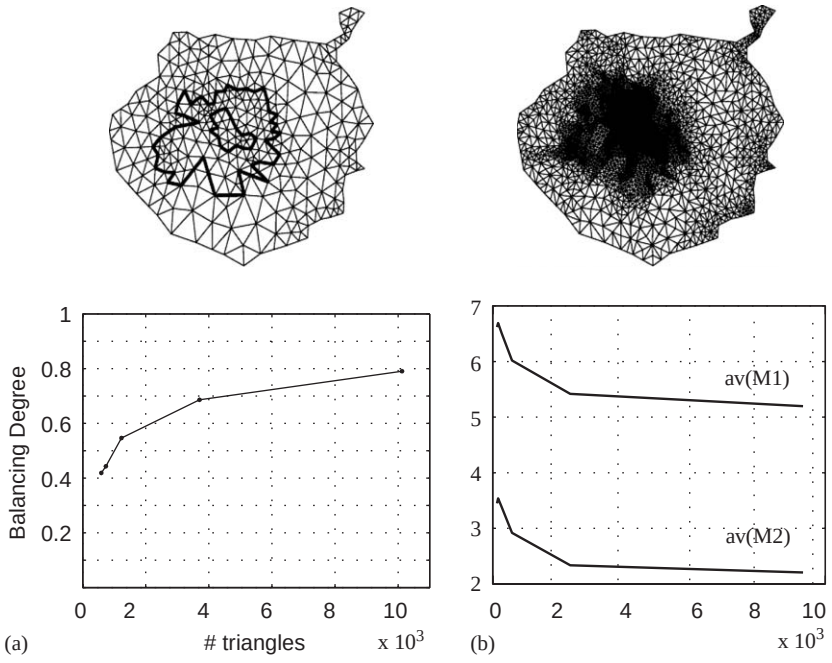

Fig. 9. Uniform 4T-LE refinement in a subregion.

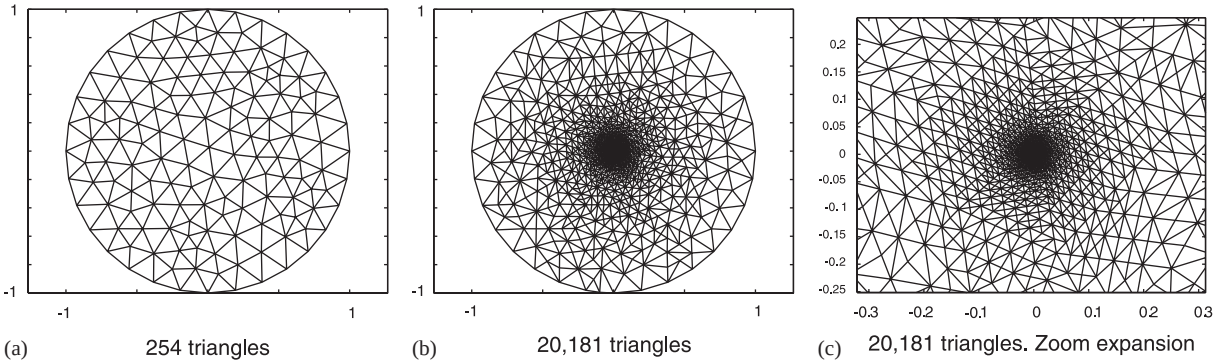

Fig. 10. Point singularity mesh refinement. (a) 254 triangles, (b) 20 181 triangles, (c) 20 181 triangles. Zoom expansion.

4.3.1. Point singularity

The test problem is the Green's function approximation for a point source at the centre of a circular disc. The disc is discretized using a Delaunay scheme to give the initial mesh of well-shaped cells in Fig. 10(a). The tolerance for refinement is 0.001 based on the flux-jump indicator in [11] and the mesh after several AMR steps is shown in Fig. 10(b) together with a zoom 'expansion' near the singular point, Fig. 10(c). There is a contracting subregion containing the singular point that is automatically selected and refined during the AMR process. The balancing degree B and averages are sketched in Fig. 11. The scheme performs well with $\mu(M1)$ and $\mu(M2)$ close to the uniform grid limits.

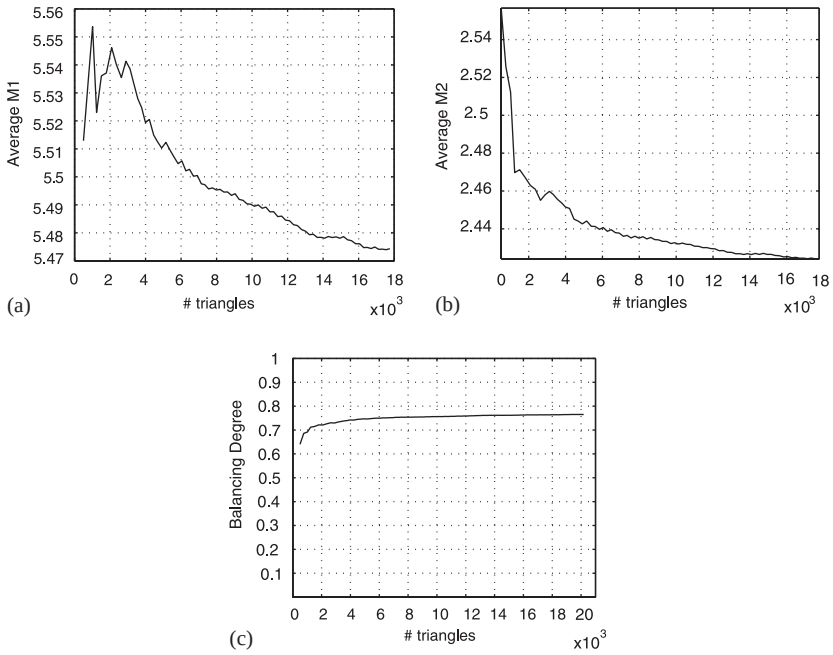

Fig. 11. Point singularity. $M1$ and $M2$ averages and balancing degree.

4.3.2. Convection–diffusion boundary layer problem

The linear convection–diffusion equation

$$-\varepsilon\Delta u + u_x + u_y = 0 \tag{12}$$

on $[0, 1] \times [0, 1]$ with u specified on the boundary to interpolate the exact solution

$$u(x, y) = \frac{e^{\frac{x}{\varepsilon}} - 1}{e^{\frac{1}{\varepsilon}} - 1} + \frac{e^{\frac{y}{\varepsilon}} - 1}{e^{\frac{1}{\varepsilon}} - 1} \tag{13}$$

and $0 < \varepsilon \ll 1$, has boundary layers of order $O(\varepsilon)$ adjacent to $x = 1$ and $y = 1$. The problem was discretized using piecewise-linear continuous triangular element basis functions on a conforming level zero mesh. The standard Galerkin scheme is used to solve the problem with $\varepsilon = 0.1$ (despite the expected oscillatory behavior on coarse meshes). The error indicator is the flux jump indicator of Johnson [11].

4.3.2.1. Ill-shaped initial mesh. The initial mesh is the same pattern as in Fig. 7 and the adaptively refined mesh with error indicator tolerance $Tol = 10^{-7}$ using 4T-LE is shown in Fig. 12. The averages $\mu(M1)$ and $\mu(M2)$ and the balancing degree evolution are graphed in Fig. 12.

Next, hybrid 4T-LE and 4T-SS are simultaneously used for AMR from the same ill-shaped uniform mesh. The averages $\mu(M1)$ and $\mu(M2)$ and the balancing degree evolution are quantitatively the same as in Fig. 12.

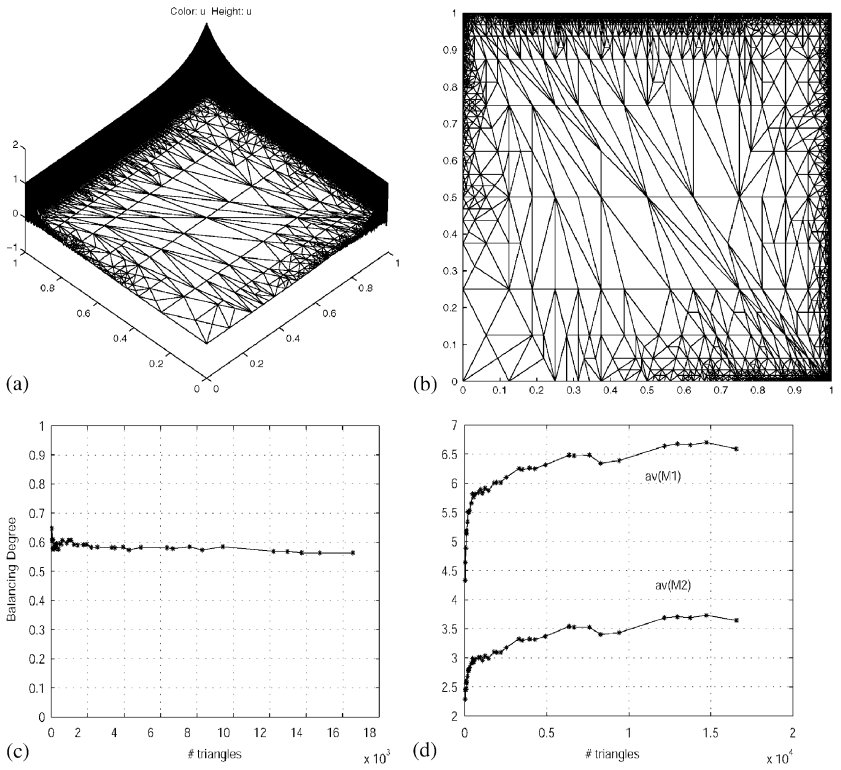

Fig. 12. Convection–diffusion problem. Ill-shaped initial mesh.

4.3.2.2. Coarse mesh in a square domain. This case considers an initial mesh with 8 right triangles and the adaptively refined mesh using 4T-LE. At any stage all elements with error indicator value within 75% of the maximum error indicator are marked for refinement. The averages $\mu(M1)$, $\mu(M2)$ and the balancing degree evolution are graphed in Fig. 13.

5. 3-D partial results

The extension of the LE propagation algorithm and results to the 3-D case is not straightforward. The problem of obtaining quality meshes in higher dimensions is much harder than in two dimensions [12]. We now use as the local subdivision strategy, the 8-tetrahedra longest-edge (8T-LE) partition which is the natural extension to 3-D of the 4T-LE triangle partition [13,14]. Note that, adjacent elements now share faces and edges rather than simply edges, and the complexity increases significantly. Two numerical experiments are next provided. In these examples we perform several stages of uniform 8T-LE refinement and for each mesh level we choose a set of interior tetrahedra in which we compute the extent $M1$ of the propagation refinement zone.

The first numerical experiment considers uniform recursive subdivision of an initial Liu–Joe canonical tetrahedron [15]. This tetrahedron has the remarkable property that its 8T-LE partition yields eight

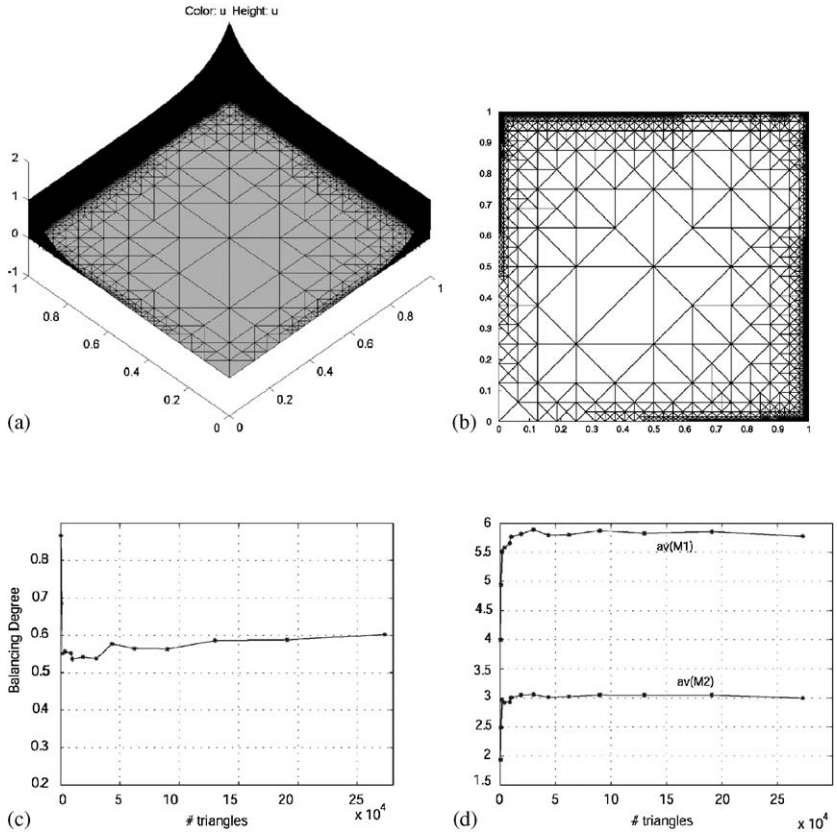

Fig. 13. Convection–diffusion problem in a coarse mesh.

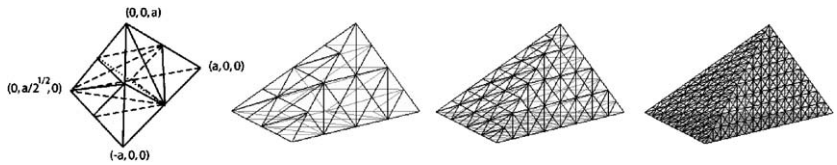

Fig. 14. Four stages of 8T-LE refinement on the Liu–Joe initial tetrahedron.

sub-tetrahedra similar to the original one, and also that 3-D space can be filled by copies of one of these tetrahedra.

In this experiment global 8T-LE refinement was performed through a few mesh levels with the finest mesh containing 262,144 tetrahedra and 47,905 nodes (e.g. see Fig. 14). For each mesh level we choose a set of interior tetrahedra and compute for every one the $M1$ value, resulting in $\mu(M1) = 75$. Note that these tetrahedra are all similar and, therefore, the value of $M1$ is the same for each 'interior' element. Fig. 15 shows the set of tetrahedra comprising the propagation refinement zone in 3-D for an interior tetrahedron with $M1(t) = 75$ in the finest mesh.

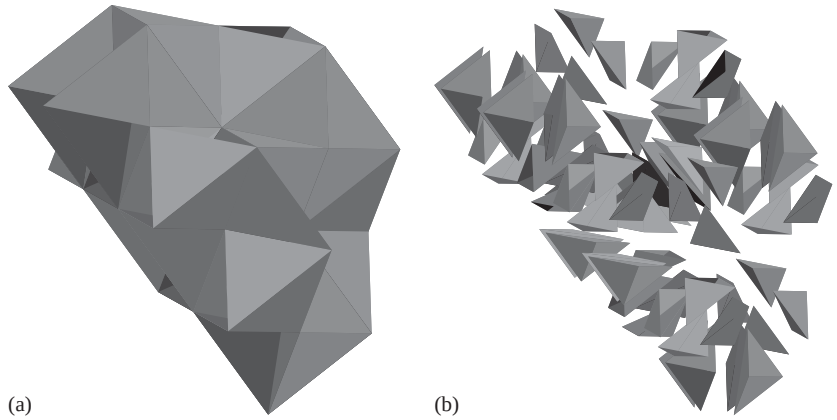

Fig. 15. (a) Set of tetrahedra in $V_C(t)$ in the sixth mesh level and (b) exploded tetrahedra set.

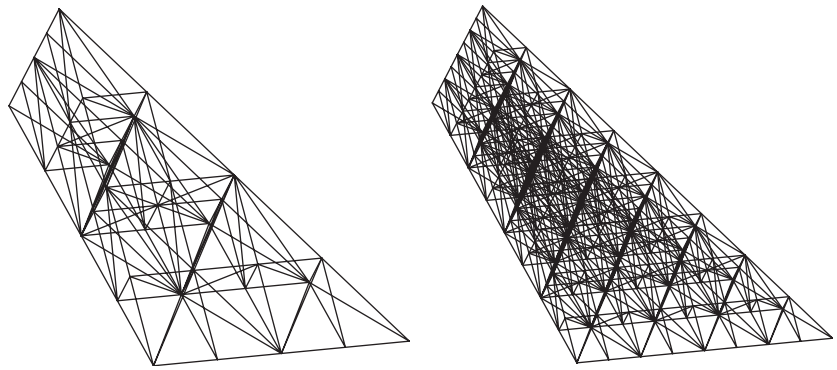

Fig. 16. Right tetrahedra. Second and third refinement stages.

For the second experiment in 3-D we consider refinement of a single *right-type* tetrahedron. A tetrahedron t is said to be a *right-type tetrahedron*, if its four faces are right triangles. For any right-type initial tetrahedron t, the iterative (8T-LE) partition of t yields a sequence of right-type tetrahedra. At most only three dissimilar tetrahedra are generated and hence the non-degeneracy of the meshes is proved [16]. After six refinement mesh levels we compute $\mu(M1) = 47$ and observe that it remains constant in each subsequent mesh considered. Fig. 16 shows the second and third refinement mesh level:

The above numerical experiment shows that $\mu(M1)$ is decreasing as the mesh is refined but it appears that the asymptotic behavior of $\mu(M1)$ has not yet been determined.

6. Conclusions and remarks

We first analyze the asymptotic balancing degree $B(\tau)$ of meshes generated by recursive uniform 4T-LE and 4T-SS refinement. Numerical tests with an initial poor triangulation confirm that balancing

degree $B(\tau) \rightarrow 1$ as refinement proceeds. This also implies that in this context the propagation path parameters $\mu(M1)$ and $\mu(M2)$ asymptotically 'improve'. The average $\mu(M1)$ tends to 5 and $\mu(M2)$ tends to 2.

Local 4T-LE/4T-SS refinement in AMR is not as well behaved. These is a 'trade-off' between similar trends due to repeated local refinement in subregions, layers or near singular points and the progressive nature of secondary refinements as the AMR scheme scales into the zone of interest. A rigorous cost estimate is difficult to ascertain. Clearly, it is proportional to the number of elements locally refined and to the average secondary refinement zone. It follows that the cost remains small relative to the other solve operations. The presence of a modest secondary refinement zone promotes quasi-uniformity of a well graded mesh.

We have included numerical results of some preliminary 3-D studies for tetrahedral elements that show the behavior of $\mu(M1)$ under refinement of a single tetrahedron using the analogous 8T-LE local subdivision. The 8T-LE scheme requires consideration of many more propagation paths and more complicated subdivision patterns [13,14] than in the 2-D case with 4T-LE. This makes both analysis and numerical experimentation a challenge and questions such as the asymptotic behavior of $\mu(M1)$ remain open.

Acknowledgements

This research has been partially supported by Sandia National Laboratory project #56522 and Gobierno de Canarias grant PI2003/35.

References

[1] M.C. Rivara, M. Vemere, Cost analysis of the longest-side (triangle bisection) refinement algorithm for triangulation, Eng. Comput. 12 (1996) 224–234.
[2] I.G. Rosenberg, F. Stenger, A lower bound on the angles of triangles constructed by bisecting the longest side, Math. Comput. 29 (1975) 390–395.
[3] M.T. Jones, P.E. Plassmann, Adaptive refinement of unstructured finite-element meshes, Finite Elements Anal. Des. 25 (1–2) (1997) 41–60.
[4] J.P. Suárez, A. Plaza, G.F. Carey, Propagation path properties in iterative longest-edge refinement, in: Proceedings of the Twelfth International Meshing Roundtable'03, SANDIA Report SAND 2003-3030P, 2003, pp. 79–90.
[5] A. Plaza, J.P. Suárez, M.A. Padrón, S. Falcón, D. Amieiro, Mesh quality improvement and other properties in the four-triangles longest-edge partition, Comput. Aid. Geom. Design. 21 (4) (2004) 353–369.
[6] M.C. Rivara, G. Iribarren, The 4-triangles longest-side partition of triangles and linear refinement algorithms, Math. Comput. 65 (216) (1996) 1485–1502.
[7] M.C. Rivara, New mathematical tools and techniques for the refinement and/or improvement of unstructured triangulations, in: Proceedings of the Fifth International Meshing Roundtable'96, SANDIA Report SAND 96-2301, 1996, pp. 77–86.
[8] T. Linss, H.-R. Roos, R. Vulanovic, Uniform pointwise convergence on shishkin-type meshes for quasi-linear convection–diffusion problems, SIAM J. Numer. Anal. 38 (3) (2000) 897–912.
[9] G.I. Shishkin, Grid approximation of singularly perturbed boundary value problems with convective terms, Soviet J. Numer. Anal. Math. Modelling 5 (1990) 327–343.
[10] J.L. Steger, F.C. Dougherty, J.A. Benek, in: K.N. Guia, U. Guia (Eds.), Advances in Grid Generation, volume ASME FED-vol 5, Chimera Grid Scheme, June 1983 (Chapter A).
[11] C. Johnson, Numerical Solution of Partial Differential Equations by the Finite Element Method, Studentlitteratur, Lund, 1987.

[12] S.A. Mitchell, S.A. Vavasis, Quality mesh generation in higher dimensions, SIAM J. Comput. 29 (4) (2000) 1334–1370.
[13] A. Plaza, G.F. Carey, Local refinement of simplicial grids based on the skeleton, Appl. Numer. Math. 32 (2) (2000) 195–218.
[14] A. Plaza, M.A. Padrón, G.F. Carey, A 3d refinement/derefinement combination for solving evolution problems, Appl. Numer. Math. 32 (4) (2000) 401–418.
[15] A. Liu, B. Joe, Quality local refinement of tetrahedral meshes based on bisection, SIAM J. Sci. Statist. Comput. 16 (1995) 1269–1291.
[16] A. Plaza, M.A. Padrón, J.P. Suárez, The 8-tetrahedra longest-edge partition of right-type tetrahedra, Finite Elements Anal. Des., 41 (3) (2004) 253–265.